Aster migration determines the length scale of nuclear separation in the *Drosophila* syncytial embryo

Ivo A. Telley,[1,2] Imre Gáspár,[2] Anne Ephrussi,[2] and Thomas Surrey[1,3]

[1]Cell Biology and Biophysics Unit and [2]Developmental Biology Unit, European Molecular Biology Laboratory, 69126 Heidelberg, Germany
[3]Cancer Research UK London Research Institute, Lincoln's Inn Fields Laboratories, London WC2A 3LY, England, UK

In the early embryo of many species, comparatively small spindles are positioned near the cell center for subsequent cytokinesis. In most insects, however, rapid nuclear divisions occur in the absence of cytokinesis, and nuclei distribute rapidly throughout the large syncytial embryo. Even distribution and anchoring of nuclei at the embryo cortex are crucial for cellularization of the blastoderm embryo. The principles underlying nuclear dispersal in a syncytium are unclear. We established a cell-free system from individual *Drosophila melanogaster* embryos that supports successive nuclear division cycles with native characteristics. This allowed us to investigate nuclear separation in predefined volumes. Encapsulating nuclei in microchambers revealed that the early cytoplasm is programmed to separate nuclei a distinct distance. Laser microsurgery revealed an important role of microtubule aster migration through cytoplasmic space, which depended on F-actin and cooperated with anaphase spindle elongation. These activities define a characteristic separation length scale that appears to be a conserved property of developing insect embryos.

Introduction

In developing organisms, important spatiotemporal decisions are taken. Correct positioning of the nucleus and spindle in a dividing cell is important for the fate of the daughter cells (Gönczy, 2008). In embryonic cells, this can be a challenge because cells can be up to two magnitudes larger than their metaphase spindle (Grill and Hyman, 2005; Schenk et al., 2010; Wühr et al., 2010). Massive microtubule aster growth has been shown to position the nuclei in *Xenopus laevis* eggs in preparation for cytokinesis (Wühr et al., 2010). In the case of most insects, the fertilized egg initially develops in the absence of cytokinesis (Foe and Alberts, 1983; Fleig and Sander, 1986; de Saint Phalle and Sullivan, 1996). Nuclei undergo rapid successive divisions, and, therefore, a vast number of nuclei share the same intracellular space in a syncytium. They need to be distributed throughout a large cytoplasmic volume and brought to the cell cortex to form a blastoderm embryo. But how do they distribute throughout the large embryo, and what sets their density?

In *Drosophila melanogaster*, the first 2 h of embryonic development are characterized by 13 syncytial nuclear divisions (Foe and Alberts, 1983). During the first nine divisions, nuclei divide every 8–9 min (25°C) and spread from the center throughout the interior of the embryo (Baker et al., 1993). At the end of the preblastoderm stage, typically after the ninth division, a fraction of the nuclei arrive at the cell cortex (Baker et al., 1993), where they are anchored and prepared for cellularization (Mazumdar and Mazumdar, 2002). Regular arrangement of nuclei at the cell cortex is essential for proper development (Hatanaka and Okada, 1991; Callaini et al., 1992; Megraw et al., 1999) and relies on the efficient distribution of nuclei through the preblastoderm embryo (Vaizel-Ohayon and Schejter, 1999; Rodrigues-Martins et al., 2007). In comparison with other cell types, at half a millimeter, the embryo is huge (Markow et al., 2009). Within the first nine divisions (70–80 min), the spreading of nuclei 6–8 µm in diameter through such a large volume of viscous cytoplasm cannot be explained by diffusion. An active transport mechanism is required for such a process. Earlier studies suggested that the microtubule and actin cytoskeletons both play important

The Rockefeller University Press $30.00
J. Cell Biol. Vol. 197 No. 7   887–895
www.jcb.org/cgi/doi/10.1083/jcb.201204019

JCB   887

THE JOURNAL OF CELL BIOLOGY

Figure 1. Single–*Drosophila* embryo extract recapitulates repeated nuclear divisions and distribution of nuclei in space. (A) Schematic of the embryo extraction procedure. (B) Sequence of fluorescence microscopy images of metaphase spindles in four consecutive division cycles in embryo extract, with Jupiter-GFP–labeled microtubules and Histone 2av–mRFP-labeled DNA. Dark round areas are yolk spheres. Bar, 10 µm. (C) Cycle time as a function of the cycle number for undiluted or buffer-diluted extract at 25°C. Each data point represents one experiment. In vivo data (Foe and Alberts, 1983; Foe et al., 1993) are shown in gray for comparison. (D) Plot of the metaphase spindle length for division cycles 7–9 of spindles in extract. Data points are in gray, black dots are the mean, error bars represent SD, and the number of measured spindles is shown in brackets (eight experiments). (E and F) Time course of the quantified spindle elongation (pole-to-pole distance) and DNA separation (chromosomes or nuclei) during nuclear division in extract (E) and example images (F). Bar, 5 µm. Solid and dotted lines are the mean and SD, respectively, of 15 (red) and 11 (green) observed divisions in different experiments. Anaphase onset is time 0. At the telophase–interphase transition, duplicated centrosomes of each daughter nucleus start separating (E [dashed bold] and F [bottom]), forming new poles, whereas nuclear separation levels off (red). The horizontal dashed line indicates the interphase mean nuclear diameter. (G) Time course of microtubule aster size. Error bars represent SD of astral microtubule lengths ($n \geq 28$, representative out of more than three repeats). (H) Image sequence (inverted gray values) of microtubules illustrating the cycle of aster size growth and shrinkage. Chromosomes and nuclei are schematically overlaid (red). Time is shown in minutes/seconds. Bar, 5 µm.
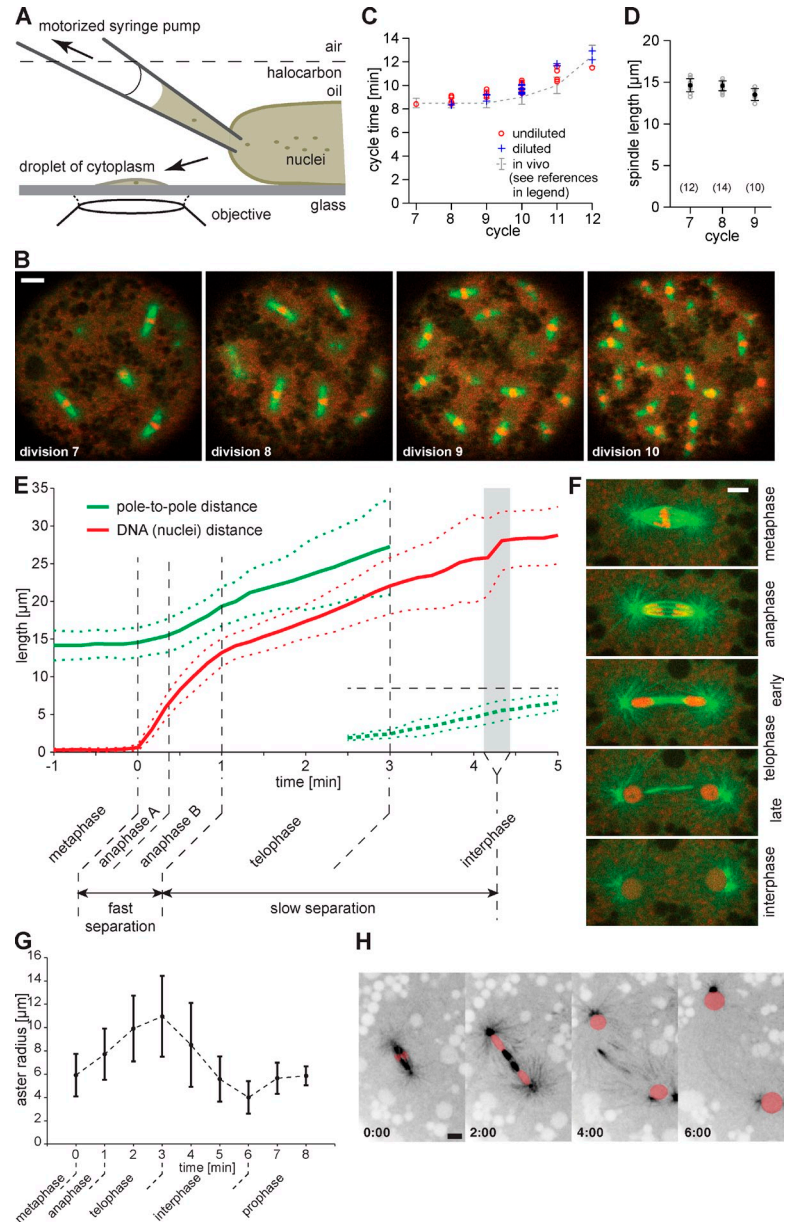
roles (Zalokar and Erk, 1976; Hatanaka and Okada, 1991; Baker et al., 1993; von Dassow and Schubiger, 1994).

Different, partly exclusive and untested models for early nuclear dispersal have been proposed, suggesting important roles of cortical factors (Bearer, 1991; Hatanaka and Okada, 1991; Reinsch and Gönczy, 1998), collective transport by a cytoplasmic streaming process (von Dassow and Schubiger, 1994), or mutual repulsion by elements of the microtubule cytoskeleton (Baker et al., 1993; Foe et al., 1993). Hence, the mechanism by which the cytoskeleton determines the correct positioning of nuclei in a syncytium is unclear, largely because visualizing nuclear movements and the associated cytoskeletal rearrangements deep inside living embryos is challenging, and tools to perturb nuclear spreading mechanically are lacking. Thus, a quantitative understanding that explains how nuclei faithfully reach the cortex at the proper density after the correct number of divisions is missing.

Results and discussion

Extracted preblastoderm cytoplasm supports autonomous nuclear division and distribution

To directly investigate the basic mechanism by which dividing nuclei distribute throughout the cytoplasm of the early *Drosophila* embryo (preblastoderm stage), we developed a cell-free assay that allows the observation of successive mitotic divisions using time-lapse fluorescence microscopy imaging. Cytoplasm was extracted from individual embryos in nuclear cycle 6 or 7 (Foe et al., 1993) during late telophase and interphase, when nuclei were intact, and extract was deposited in droplets of defined size (typically 80–100 µm in diameter and 10–30 µm in height; Fig. 1 A). Transgenically encoded fluorescent proteins marking DNA (Histone 2Av–mRFP) and microtubules (Jupiter-GFP, a microtubule-associated protein;
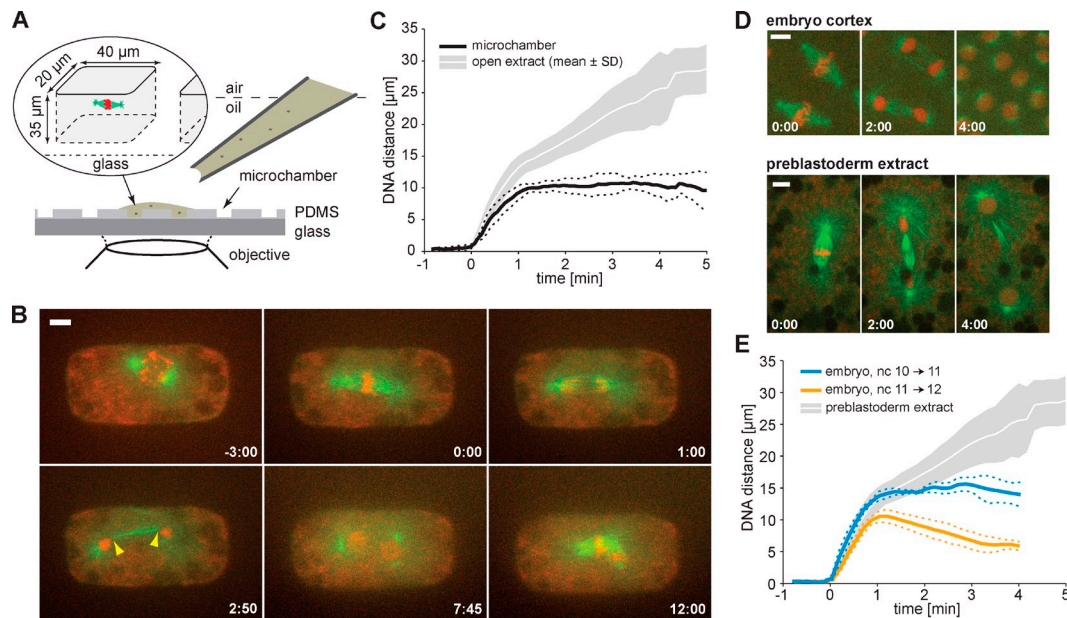
Figure 2. **Syncytial nuclear separation does not scale with available space.** (A) Schematic of spatially confining nuclei and spindles in microchambers. (B) Image sequence of a dividing nucleus (cycles 7–8) inside a microchamber. The deforming central spindle (arrowheads) suggests unaltered separation activity. In the subsequent interphase, the distance between daughter nuclei is abnormally short, leading to spindle fusion during next mitosis. Time is shown in minutes/seconds. Bar, 5 µm. (C) Distance–time plot of DNA masses during chromosome and nuclear separation in a microchamber (black) compared with unconfined extract (white line on gray background; mean ± SD; from Fig. 1 D). The solid and dotted lines are the mean distance and SD, respectively, of five experiments. (D) Images of dividing nuclei at the cortex of an intact cycle 11 (blastoderm) embryo (top) and of nuclear divisions in unconstrained early (preblastoderm) embryo extract at cycle 7 (bottom). Time is shown in minutes/seconds. Bars, 5 µm. (E) Distance–time plot of daughter DNA masses during nuclear divisions in intact blastoderm embryos (blue, division 10; orange, division 11; see D). Solid and dotted lines are the mean and SD, respectively, of 15 independent extract experiments (gray) and 5 (blue) and 10 (orange) separation measurements in two intact embryos. nc, nuclear cycle.

Morin et al., 2001; Karpova et al., 2006) were imaged, providing unprecedented detail of nuclear divisions at this developmental stage. Strikingly, repeated rapid synchronous mitotic divisions continued in the single-embryo extract (Figs. 1 B and S1 A and Video 1). Multiple divisions led to spreading of nuclei throughout the entire available space, recapitulating the distribution of dividing nuclei in fixed embryos (Baker et al., 1993). This demonstrates that homogenous nuclear distribution is an intrinsic property of the preblastoderm nucleocytoplasm and that a cortex with its associated activities is not required.

The division cycle times increased from ∼9 min in cycle 7 to ∼12 min in cycle 12 at 25°C (Fig. 1 C), consistent with previous measurements in fixed embryos (Foe and Alberts, 1983). Dilution of the extract with up to an equal volume of buffer did not affect cycle times, demonstrating the robustness of this native extract, the first in which repeated mitotic divisions occur. It represents a novel tool for studying the spatiotemporal development of rapidly dividing nuclei, and of mitosis as such, under conditions that allow full genetic, biochemical, and mechanical manipulation.

Metaphase spindle length during cycles 7–9 remained roughly constant at ∼14 µm (Fig. 1 D), lending support to the emerging principle of an upper limit for spindle size in large embryos (Wühr et al., 2008). The time course of DNA separation had two prominent phases. At anaphase onset, the duplicated chromosome masses started to separate rapidly (chromosome segregation) until they decondensed and nuclei reformed, marking the beginning of telophase. Throughout telophase, the central spindle continued to elongate, although more slowly than in

anaphase, and spindle poles associated with reforming nuclei continued to move apart (Fig. 1 E, green line). In parallel, the distance between daughter nuclei increased (Fig. 1 E, red line). Typical for syncytial divisions (Kellogg et al., 1988; Callaini and Riparbelli, 1990), centrosomes duplicated in telophase, and the new spindle poles migrated around the nucleus in interphase (Fig. 1 E, dashed bold lines) after the central spindle had disappeared (Fig. 1 F, bottom). The nuclei continued to move apart slowly even in the absence of central spindle microtubules (Videos 1 and 2). During this time, their associated microtubule asters were larger (Fig. 1, G and H). Finally, daughter nuclei reached a mean separation distance of ∼28 µm (Fig. 1 E, red line) concomitant with a decrease in astral microtubule length (Fig. 1 G). This nuclear separation distance was independent of the division cycle for noncrowded extract droplets.

Preblastoderm nuclear separation length is insensitive to spatial constraints

To investigate whether this specific distance is a hard-wired property of the preblastoderm division machinery or whether the machinery scales with available space, we exploited a major advantage of the extract assay. We confined a single nucleus within the rigid boundaries of a microchamber of dimensions similar to the separation distance (Fig. 2 A). Under these spatial constraints, individual nuclei divided, and spindles often aligned their axis along the longest chamber diameter (Fig. 2 B). The spindle substructures deformed rather than size adapted. In telophase, the midzone appeared bent, whereas the nuclei rotated, and the astral microtubules contacting the chamber walls buckled
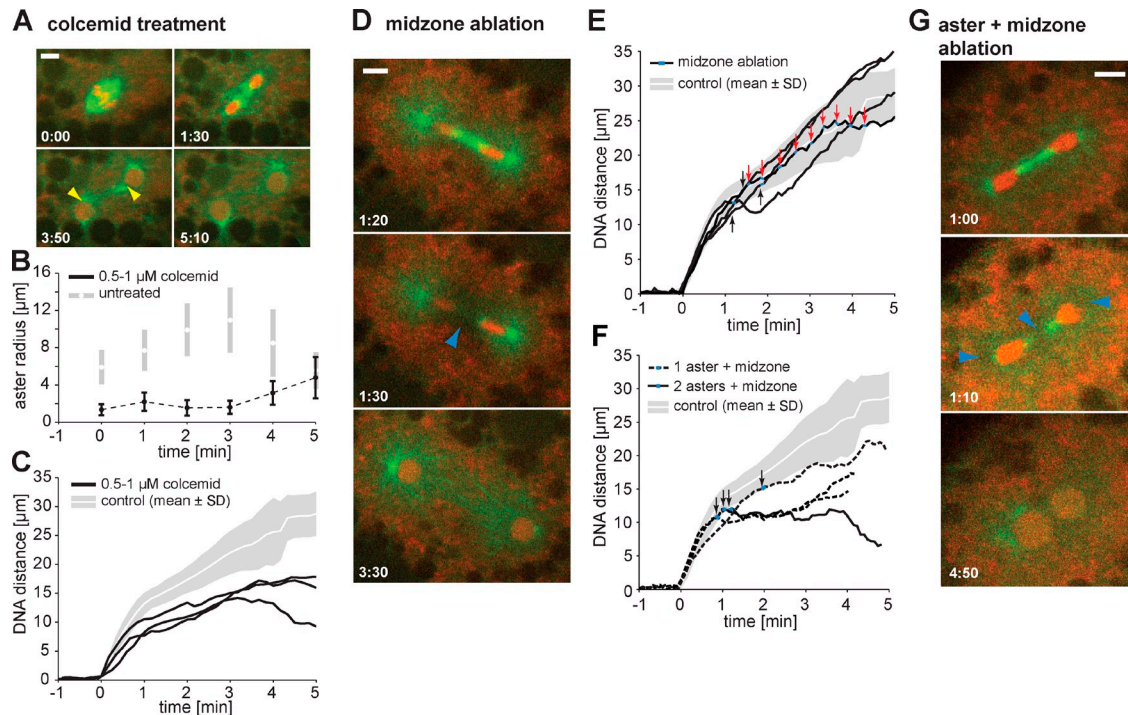
Figure 3. **Microtubule perturbation by drugs and local laser ablation reveals an important role of centrosomal asters for nuclear separation.** (A and B) Low doses of colcemid (0.5–1.0 µM) allow chromosome segregation but reduce the size of microtubule asters in preblastoderm embryo extract, as shown by fluorescence microscopy (A) and as a graph of quantified aster radius (black; $n \geq 20$, representative out of three repeats; B) compared with untreated extract (gray; from Fig. 1 G). Nuclei rotated away from the spindle axis (yellow arrowheads in A). (C) Distance–time plot of daughter DNA masses in colcemid-treated extract (solid lines) showing a significant reduction ($P < 0.001$) of both the fast and slow phase of DNA separation, as compared with the control (gray; from Fig. 1 E). (D) Fluorescence microscopy images of central spindle (midzone) ablation by a UV laser beam during telophase (blue arrowhead). (E) Graph illustrating continued nuclear separation between DNA masses (black lines and arrows indicate ablation; red arrows indicate repeated ablation). (F and G) Additional single centrosomal aster ablation caused the associated nucleus to pause, reducing nuclear separation (dashed black lines). Additional combined ablation (arrows) of both centrosomes abolished postanaphase separation (solid line and G). Each distance–time curve represents an independent experiment. DNA is shown in red, and microtubules are shown in green. Time is shown in minutes/seconds. Bars, 5 µm.

(Figs. 2 B and S1 B). This is indicative of compressive forces, most likely a consequence of the midzone generating outward-pushing forces. Consequently, DNA separation was markedly slowed down and essentially stopped at ∼10 µm after anaphase (Fig. 2 C). Neighboring nuclei in the next interphase were unnaturally densely packed. Nevertheless, the nuclei continued their mitotic program and entered a second round of division; however, the spindles exhibited severe morphological defects (Video 3). This demonstrates that preblastoderm spindles cannot adapt to reduction of available space. Their division program is presumably set to ensure that a domain of ∼28 µm is occupied by each nucleus. This differs from later-occurring divisions, when spindles are anchored at the cortex (blastoderm stage), and the available space for each nucleus decreases with each division (Figs. 2 D and S1 C). At that developmental stage, spindles reduce their size progressively (Fig. 2 E; Brust-Mascher and Scholey, 2007).

Nuclear separation is defined by actin-dependent migration of centrosome-nucleated microtubules

Central spindle microtubules are crucial for the elongation of anaphase B spindles (Sharp et al., 2000; Glotzer, 2009). It is less clear what drives the movement of syncytial nuclei after anaphase (Baker et al., 1993; Foe et al., 1993). To test a potential

role of astral microtubules, whose length reaches a maximum at the end of telophase (Fig. 1 F), we treated extract with low doses of microtubule-destabilizing drugs. Reduced astral microtubule density without a visible change of the central spindle (Figs. 3 [A and B] and S2 A and Video 4) led to a reduced separation velocity and decreased the final distance of nuclear separation after anaphase (Fig. 3 C), in contrast to treatment with buffer alone (Fig. S2 B). This suggests that in addition to the established role of central spindle microtubules in anaphase, astral microtubules contribute to the separation of the genetic material after anaphase in the preblastoderm cytoplasm despite the absence of cortical anchoring.

To dissect the contributions of the central spindle and the microtubule asters to postanaphase nuclear separation directly, we performed laser microsurgery. Remarkably, ablation of the central spindle midzone in telophase (Figs. 3 D and S3 A), even when repeated several times, did not affect subsequent nuclear separation (Fig. 3 E and Videos 5 and 6). Destruction of one centrosome, initiating rapid disassembly of the associated microtubule aster, caused its associated nucleus to pause and led to later midzone deformation (Fig. S3 B). Thus, after anaphase, nuclear separation appears to be mainly driven by microtubule aster migration and supported by midzone elongation. This predicts that only multiple ablations can stop nuclear separation. Indeed, simultaneous ablation of the midzone and one centrosome
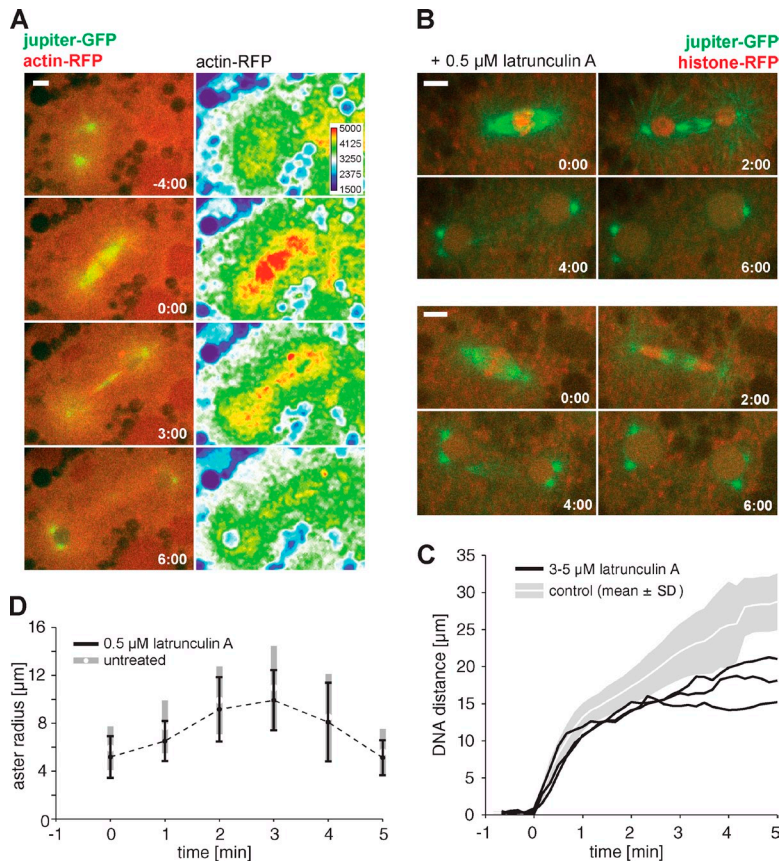
Figure 4. An F-actin network supports nuclear separation. (A, left) Overlay fluorescence microscopy images of actin (red) and microtubules (green) during nuclear separation in extract. (right) Heat map of the red channel showing actin concentrating in the spindle and asters. (B) Two examples of confocal microscopy time-lapse images of nuclear division while actin filament turnover was inhibited using latrunculin A. (A and B) DNA is in red, and microtubules are in green. Time is shown in minutes/seconds. Bars, 5 µm. (C) Inhibiting actin filament turnover reduced final separation distance (black lines) by significantly (P < 0.001) slowing down postanaphase movement of daughter nuclei, whereas chromosome segregation in anaphase is unaffected (P = 0.111). Each curve represents an independent experiment (gray; from Fig. 1 E). (D) The aster size in latrunculin A–treated extract (black; $n \geq 20$, representative out of three repeats) was essentially as in untreated extract (gray; from Fig. 1 G).

dramatically reduced nuclear separation, except for some residual movement caused by the still-intact aster of the second nucleus (Fig. 3 F, dashed lines). Finally, when the midzone and both asters were removed, separation stopped completely, and the nuclei collapsed back to the spindle center (Fig. 3 G).

What do asters pull on in the syncytium? In the absence of a cortex, astral microtubules may anchor to an actin filament network within the cytoplasm (Hatanaka and Okada, 1991; Foe et al., 1993; von Dassow and Schubiger, 1994; Reinsch and Gönczy, 1998). We visualized both actin and microtubules in extract by mixing cytoplasm from actin-RFP and Jupiter-GFP embryos. Actin concentrated around the spindle and its asters from metaphase to telophase (Fig. 4 A and Video 7). Inhibition of F-actin turnover with latrunculin A reduced DNA separation after anaphase (Fig. 4 [B and C] and Video 8), whereas aster size was unchanged (Fig. 4 D). These results suggest that F-actin plays at least an indirect role in supporting aster movement by forming a reference network for anchoring.

Hence, two distinct mechanical activities, generated by F-actin–dependent aster migration and central spindle elongation, cooperate to separate nuclei in the syncytium (Fig. 5 A). Despite lacking cortical interactions, preblastoderm asters play a decisive role. The important role of centrosome-nucleated microtubule asters explains the strict requirement of centrosomes in early *Drosophila* development (Dix and Raff, 2007; Rodrigues-Martins et al., 2008), unlike in later developmental stages when centrosomes are dispensable (Megraw et al., 2001; Basto et al., 2006). Movement of asters not in contact with the cortex might be a general feature of very large embryonic cells

(Hamaguchi and Hiramoto, 1986; Wühr et al., 2010), whereas cortical anchors are key in smaller cells (Grill et al., 2003; von Dassow et al., 2009).

Single-embryo extract observations compared with previously proposed models

Visualizing nuclear movements in living preblastoderm embryos is challenging as a result of the large size of the embryo and the considerable amount of yolk. Past studies using either live differential interference contrast or fluorescence microscopy of embryos fixed at different times reported two phases of collective nuclear movements during the early syncytial cleavages. Spreading along the anterior–posterior embryo axis (axial expansion, cycles 4–6; von Dassow and Schubiger, 1994) required the actin cytoskeleton (Zalokar and Erk, 1976; Hatanaka and Okada, 1991) and was thought to be driven by cytoplasmic flow (von Dassow and Schubiger, 1994). Nuclear displacement toward the embryo cortex (cortical migration, cycles 7–9; Foe and Alberts, 1983; Baker et al., 1993) occurred episodically, during telophase and interphase of each division (Foe and Alberts, 1983), and required microtubule function (Baker et al., 1993). Thus, separation of daughter nuclei by the central spindle machinery during telophase (Foe et al., 1993) and additional mutual repulsion of nondaughter nuclei by plus end–directed kinesins pushing astral microtubules apart (Baker et al., 1993) were proposed to drive cortical migration. Whether or not the cortex is key for both phases has remained unclear.

Using single-embryo extract, we have revealed the existence of an autonomous mechanism for nuclear spreading independent
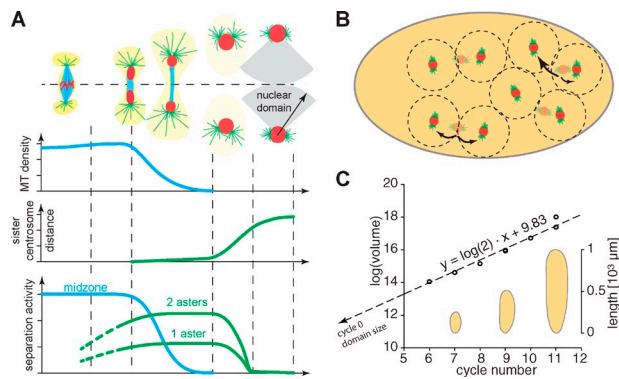
Figure 5. **The length scale of separation is conserved among different species.** (A) Schematic illustration of nuclear separation (top) and proposed activities (bottom). After chromosome segregation in anaphase, the central spindle disassembles (blue), and microtubule (MT) asters (green) linked to F-actin (yellow) transport daughter nuclei further apart. This transport continues until sister centrosomes have reached opposite sides of the nucleus (green line in middle graph). This diametric centrosome positioning cancels migration of the sister asters, and nuclear movement ceases. The internuclear distance defines a nuclear domain (gray) of characteristic size. (B) Scheme of a hypothetical, small-sized syncytium with four dividing nuclei, illustrating the principle of nuclear distribution. The number of divisions and the size of the nuclear domain (dashed circles) determine when nuclei reach the cortex by filling cytoplasmic space. (C) Logarithm of embryo volume as a function of the observed number of preblastoderm divisions for different insect species undergoing a syncytial phase of development in embryos of different size (see Table 1). Regression analysis predicts a domain size in the range of 28.1 and 31.3 µm with 95% confidence. For three species, an embryo is drawn to scale and positioned on the x axis.

of cytoplasmic streaming and cortical cues (Fig. 1 B and Videos 1 and 2). Yolk particles were pushed away by separating nuclei (Video 2), arguing against cytoplasmic flow transporting nuclei (von Dassow and Schubiger, 1994). Astral microtubules contribute to nuclear separation in telophase and provide the only source of movement in interphase (Fig. 3). This is in line with the reported episodic cortical migration (Foe and Alberts, 1983) and reports of centrosomes and associated microtubules migrating to the embryo cortex in the absence of nuclear divisions (Freeman et al., 1986; Raff and Glover, 1989). However, autonomous aster movement argues against nuclear migration driven solely by central spindle pushing (Foe et al., 1993). The reported ringlike arrangement of the most outer nuclei seen in fixed embryos (Baker et al., 1993) might be a consequence of an increasing density of the actin cytoskeleton toward the cell cortex (von Dassow and Schubiger, 1994; Foe et al., 2000; Riparbelli et al., 2007), possibly generating an exclusion zone that promotes ordered, directional expansion (Field and Lénárt, 2011). Gradual disassembly of an actin gel in this exclusion zone might assist the final stages of cortical migration (Hatanaka and Okada, 1991), requiring additional mechanisms, such as microtubule-based actin remodeling (Waterman-Storer et al., 2000), that are absent in our simplified cell-free system. Improved in vivo imaging should resolve this question in the future.

The principle of constant nuclear domain size in syncytial development

The early *Drosophila* embryo extract exemplifies how the length scale for the distance between multiplying nuclei is set in a syncytium. The nuclear division machinery does not adapt to space

constraint. Instead, the biochemical activities of the preblastoderm cytoplasm define a characteristic separation distance of nuclei, or a nuclear domain size (Fig. 5 A), reminiscent of a concept formulated earlier for plants (Mazia, 1993; Baluska et al., 2004). It is interesting to compare the characteristic nuclear domain size of ∼28 µm diameter in early *Drosophila* embryo extract (Fig. 1 E) with the total available embryo volume assuming ellipsoidal shape (0.51 mm long and 0.18 mm wide; Markow et al., 2009). Assuming an even distribution of spherical nuclear domains in the embryo volume (Fig. 5 B), our calculations show that after nine divisions, these domains fill the embryo volume completely (see Materials and methods). At this stage, some nuclei remain in the interior of the embryo (for example, see Fig. 1 in Baker et al. [1993]), whereas the majority is in contact with the cortex. Remarkably, now the division program changes, and nuclei continue to divide while anchored at the cortex of the blastoderm embryo (Schejter and Wieschaus, 1993). Hence, the length scale of nuclear separation appears to be perfectly adjusted to the requirements of nuclear distribution before the blastoderm stage, setting the basis for later cellularization.

Different insect species may have embryos with different sizes. How does embryo size relate to nuclear separation distance? This distance could either scale with embryo size if the number of nuclear cycles was constant for embryos of different size or the number of divisions required for nuclei to reach the cortex could scale with embryo size, keeping the nuclear separation distance constant. Comparison of our data with the literature argues strongly for the latter scenario. Assuming a constant separation distance of ∼28 µm (as measured in *Drosophila* extract), our simple model does not only correctly predict the number of divisions required to fill the *Drosophila* embryo but also larger and smaller insect embryos that are known to have fewer or more division cycles before cortical anchoring, respectively (Table 1, middle columns; Anderson, 1962; Raminani and Cupp, 1975; Bull, 1982; Fleig and Sander, 1986; Perondini et al., 1986; Sommer and Tautz, 1991; de Saint Phalle and Sullivan, 1996). Inversely, relating embryo dimensions and the observed number of divisions for nuclei to arrive at the cortex, our model predicts a roughly constant nuclear domain size of ∼29 µm for several species (Table 1, last column), inferred from a remarkably linear correlation between the logarithm of embryo volume and the reported number of preblastoderm divisions (Fig. 5 C). Therefore, the length scale of nuclear separation in the early syncytial embryo appears to be conserved, whereas the number of divisions required for nuclei to reach the cortex scales with embryo size. This shows how the scaling of a subcellular structure relates to the developmental program of an entire organism. Our simple model appears to reflect a general principle of nuclear positioning in a syncytium.

Materials and methods

Fly strains
w^{1118};;P{PTT-GA} Jupiter^{G00147} flies (a gift from A. Debec, Université Pierre et Marie Curie, Paris, France; Morin et al., 2001; Karpova et al., 2006) were crossed with w^{1118};;P{His2Av–mRFP1} (stock no. 23650; Bloomington Stock Center) to generate w^{1118};;P{PTT-GA} Jupiter^{G00147}, P{His2Av–mRFP1} recombinant progeny. The resulting stock was homozygous viable.

Table 1. Summary of dimensions and division cycles in the syncytial embryo of eight different species

Species	References	Embryo size (length; width)	Nuclei at cortex after (divisions)		Domain size calculated[b]
			Calculated[a]	Observed	
		µm			µm
Sciara coprophila[c]	de Saint Phalle and Sullivan, 1996	200; 110	6.35	6	30.4
Bradysia tritici	Perondini et al., 1986	250; 130	7.16	7	29.0
Mormoniella vitripennis	Bull, 1982	370; 140	7.93	8	27.6
Drosophila melanogaster	Foe and Alberts, 1983; Markow et al., 2009	510; 180	9.12	9	28.8
Aedes aegypti[d]	Raminani and Cupp, 1975	620; 160	9.06	9	28.4
Dacus tryoni[e]	Anderson, 1962	975; 190	10.21	10	29.4
Musca domestica	Sommer and Tautz, 1991	1,000; 260	11.2	11	29.0
Apis mellifera	Fleig and Sander, 1986	1,400; 300	12.05	11	35.7

[a]Assuming a domain size of 28 µm, as measured in this study.
[b]Assuming the observed number of divisions for nuclei to reach the cortex.
[c]Embryo dimensions were measured in the pictures presented in reference.
[d]Number of divisions estimated from cycle time and time for arrival of nuclei at the cortex.
[e]Number of divisions deduced from time point of appearance of pole buds and formation of pole cells.

The strain w^{1118};*UAS-actin-RFP* (stock no. 24778; Bloomington Stock Center) was crossed with w^{1118};*P{oskGal4}* flies to generate progeny that expressed actin-RFP in the germline. For the generation of the w^{1118};*P{oskGal4}* line, a 1,786-nucleotide-long fragment including 1,743 nucleotides of the *oskar* promoter adjacent to the transcription start, the 15-nucleotide-long *oskar* 5′ untranslated region, and 24 nucleotides of *oskar* coding sequence was amplified using the primers 5′-tatcG|AATTCGCTGCTGGTAA-3′ and 5′-gcagG|-GTACCACTTGTGACTGCGGCCTT-3′ to introduce EcoRI and Acc65I restriction sites on the 5′ and 3′ of the fragment, respectively, and to remove the start code of *oskar* (the vertical lines represent the restriction site, and lowercased letters indicate the upstream overhang to improve site recognition). This regulatory fragment was cloned to pCaSPeR4 (Drosophila Genomics Resource Center) using the appropriate restriction enzymes. The coding sequence of the Gal4-VP16 transactivator fused with the 3′ untranslated region of αTub84B and *Hsp70* (Pignoni and Zipursky, 1997) was amplified using 5′-ttagG|GTA-CCATGAAGCTACTGTCTTCTATC-3′ and 5′-actaC|TGCAGATATCGAATTCG-AAGTTC-3′ primers and was cloned downstream of the *oskar* regulatory fragment using Acc65I and PstI restriction enzymes. The resulting construct was used to generate transgenic animals in a *P* element–mediated transgenesis. Several transgenic lines with individual insertions on the X, second, and third chromosome were recovered. Fly stocks were maintained on standard apple-maize medium in vials at 18°C.

Embryo collection and sample preparation
We followed established procedures (Schubiger and Edgar, 1994) of fly husbandry, initiating egg laying and collecting synchronously developing embryos, except that we made timed collections every 70 min (25°C). Young embryos expressing actin-RFP were collected 30 min after egg laying. Embryos were dechorionated by immersing them in ~5% sodium hypochloride (Merck & Co., Inc.) for 10–20 s. After rinsing with water, we aligned and immobilized embryos in one row on a round cover glass and covered them with halocarbon oil (Voltalef-10S).

Pipette production and flow system
Pipettes for extracting cytoplasm were produced from borosilicate tubing with a 0.75-mm inner diameter and a 1.0-mm outer diameter using a vertical pipette puller (PC-10; Narishige). The tip of the pipette was cut manually with a razor blade such that the outer diameter of the tip was roughly 50 µm and contained a sharp edge. Fine pipettes for buffer droplet production were made from tubing with a 0.50-mm inner diameter. After pulling, the final aperture of the tip was 1–2 µm. Before pulling, glass tubing was incubated in vapor of chlorotrimethylsilane (Sigma-Aldrich) for 5 min. The coarse pipette for embryo extraction was connected with Teflon tubing to a gas-tight syringe (1750TLL-SAL; Hamilton Company) driven by a motorized pump (SP210CZ; World Precision Instruments). The micropipette for buffer droplet production was seal mounted to the pipette holder of a manual, oil-driven microinjector (CellTram Oil; Eppendorf). Each pipette was mounted to a three-axis micromanipulator on the microscope platform (MI-10010; Sutter Instrument).

Micromanipulation
The frame of an inverted, motorized light microscope (IX-81; Olympus) was fixed on a vibration-free optical table. Independent of the motorized stage (H117 ProScan; Prior Scientific), a second platform was connected to the microscope frame and to the optical table (Thorlabs, Inc.). Two three-axis motorized manipulators (MP-285; Sutter Instrument) were mounted on this platform close to the optical axis of the microscope, leaving space for the upright condenser. Micromanipulators were operated with a three-axis rotational handle (ROE-200; Sutter Instrument) linked to the control unit (MPC-200; Sutter Instrument). Manipulations using the glass pipettes were performed in transmission mode using a 20× UPlanApo 0.8-NA oil objective (Olympus), a long working distance 0.55-NA condenser (Olympus), and a polarizer and analyzer in crossed configuration.

Microscopy system
Spinning-disk confocal imaging (Andor Technology) was performed using 491- and 561-nm laser lines for excitation, a confocal scanner (5,000 rpm; CSU-X1; Yokogawa Electric Corporation), an emission filter wheel (Lambda 10B; Sutter Instrument), and an electron-multiplying charge-coupled device camera (iXon, DU-885; Andor Technology) with an 8-µm pixel size. We used either a 20× UPlanApo 0.8-NA oil objective or a 40× UPlanFL 1.3-NA oil objective (both Olympus) for time-lapse imaging (100-ms exposure; 5, 10, or 20 s between frames) of the nuclear divisions in extract and in intact blastoderm embryos. Except during UV laser ablation, we magnified the field of view with the built-in 1.6× optovar. iQ software (Andor Technology) was used to control the microscope and for image acquisition.

Single-embryo extract assay
The cell cycle stage of embryos was determined using confocal fluorescence microscopy at 20× magnification. Typically, preblastoderm embryos that were in late anaphase/telophase of nuclear cycle 6 or 7 were chosen for extraction (Foe and Alberts, 1983). Cycle 6 (32 nuclei) was detected by observing >16 Jupiter-GFP signal patches from telophase spindles in the interior of the embryo. In cycle 7, when nuclear migration starts, the spindles on the side of the embryo facing the objective became more clearly visible. We verified our method of cycle stage detection by counting cycles (without extraction) until nuclei reached the cortex (cycle 10). For extraction, the vitelline membrane of a selected embryo was punctured with a pipette, and suction from inside the embryo was started immediately. Thereafter, the microscope stage was moved, and small droplets of cytoplasm (volume of 10–500 pL) were placed on the glass surface. As extraction was performed during telophase or the following interphase, time-lapse imaging typically started in late interphase or prophase. For imaging both actin and microtubules, extract droplets from embryos expressing actin-RFP were mixed with cytoplasm from embryos expressing Jupiter-GFP at a ratio of roughly 1:1. All experiments were performed at 25°C.

Production of microchambers
Arrays of microchambers of 20 × 40 and 30 × 30 µm were made in a single layer of polydimethylsiloxane (PDMS) cast from a master mold that

was fabricated using soft lithography techniques (Simonnet and Groisman, 2006). To make the PDMS microchambers, a layer of PDMS prepolymer (Sylgard 184; Dow Corning) was spin coated onto the master mold and baked in an oven at 70°C for 1 h. The thickness of the PDMS layer was chosen such that it covered minimally the feature height. The region containing the microchambers was cut out, peeled off the mold using forceps, and placed on a cover glass with the feature side up.

Extract dilution and drug treatment
Using a fine pipette, small droplets (20–50 µm in diameter) of buffer (20 mM Hepes, pH 7.8, 100 mM KCl, 2 mM MgCl$_2$, and 1 mM EGTA) or buffer containing a drug (nocodazole, colcemid, and cytochalasin D were diluted 1:1,000 and latrunculin A 1:100 from a stock in DMSO) were positioned next to the immobilized embryos. Then extract was added aiming at dilutions of ∼1:1. Diluted extract containing up to 1% DMSO preserved nuclear cycling (Fig. 1 C).

Laser ablation
The laser ablation system was initially designed by G. Heuvelmann and L. Hufnagel (European Molecular Biology Laboratory, Heidelberg, Germany). In brief, a 355-nm pulsed laser (15 µJ, 1-ns pulse width, 2.5 kHz; FT 55-355-Q; CryLas GmbH) was coupled into the light path using a dichroic mirror placed between the microscope and spinning-disk unit. The intensity of the expanded beam was controlled with a rotational polarizer after passing through a half-wave plate. A scanning galvano-mirror system (Thorlabs, Inc.) allowed high-speed positioning of the beam in x and y directions. The system was controlled with an in-house written plug-in for iQ software. Laser power was adjusted and tested by irradiating nuclei or chromosomes in extract, causing the nucleus to burst and chromosomes to melt and arrest mitosis, which confirmed that we do not observe bleaching only.

Data analysis
Basic image sequence analysis was performed in ImageJ (National Institutes of Health). For the measurement of unconfined nuclear separation (Fig. 1 D), experiments with one to three nuclei per extract droplet were considered (noncrowded situation). The centers of chromosome masses and nuclei were tracked manually during nuclear division and separation. Tracking error (±3 pixels < 0.5 µm) was estimated by repeated tracking and was smaller than the variability between experiments. The Euclidean distance between tracked objects was calculated and plotted as a function of time. For averaging curves from several experiments, we calculated the arithmetic mean and SD from data points that belonged to nonoverlapping time windows (bin size of 10 s) and plotted mean ± SD against the center of the time window. The mean aster size (radius) was determined by manually measuring the length of all visible astral microtubules and pooling the data. For calculations and graphs, we used MATLAB (MathWorks). A heat map of the actin-RFP signal was generated using ImageJ (median filter with a width of 3 pixels).

Statistical test
To test for differences in postanaphase nuclear separation dynamics between control and test experiments (drug treatment and dilution), all DNA distance–time curves from individual experiments were pooled, and a multiple linear regression was performed between the time points 1 min (end of anaphase) and 5 min using the software package R. The abscissa was shifted so that time point 1 min was the new origin. The presence and absence of a treatment were described with a categorical factor g in the model

$$y = b_1 + m_1 x + g(b_2 + m_2 x),$$

whereby $g = 0$ represents control, and $g = 1$ represents test conditions (x axis, time; y axis, distance). The statistical significance level of the parameter b_2 defines whether chromosome separation at the end of anaphase is different between the two conditions, whereas m_2 defines whether the slopes, and hence the dynamics, of the postanaphase separation are different. The significance level was set at $P = 0.05$ before testing.

Model calculation
Each nucleus occupies a nuclear domain represented as a sphere with diameter d. The volume of an embryo is approximated as a rotation ellipsoid with length L and cross-sectional diameter D. We assume tight packing of spherical domains; hence, the effective volume occupied by the spheres is $\pi/\sqrt{18} = 74\%$. Then, if n divisions produce 2^n nuclei, the calculated number of divisions to fill the entire embryo is

$$n = \ln\left(\frac{\pi L D^2}{\sqrt{18}d^3}\right)/\ln(2),$$

where ln is the natural logarithm. Similarly, the nuclear domain size d can be calculated from the number of divisions, n. Consequently, the logarithm of the embryo volume depends linearly on n for a constant nuclear domain size d.

Online supplemental material
Fig. S1 compares nuclear separation in unconfined and confined extract as well as at the cortex in vivo. Fig. S2 shows that a small dose of nocodazole reduces nuclear separation distance and that buffer-diluted extract supports normal nuclear separation. Fig. S3 shows an intensity profile during UV laser ablation of the central spindle and illustrates the pausing of a nucleus whose associated aster has been removed. Video 1 shows a nucleus in extract undergoing five division cycles. Video 2 illustrates nuclear movement during interphase. Video 3 shows nuclear separation in confined space, and Video 4 shows its reduction in the presence of colcemid. Videos 5 and 6 show nuclear separation during single and repeated UV laser ablation, respectively, of the central spindle. Video 7 illustrates actin accumulation during a nuclear division, and Video 8 shows reduced nuclear separation when inhibiting F-actin turnover. Online supplemental material is available at http://www.jcb.org/cgi/content/full/jcb.201204019/DC1.

References

Anderson, D.T. 1962. The Embryology of *Dacus tryoni* (Frogg.) [Diptera, Trypetidae (=Tephritidae)], the Queensland Fruit-Fly. *J. Embryol. Exp. Morphol.* 10:248–292.

Baker, J., W.E. Theurkauf, and G. Schubiger. 1993. Dynamic changes in microtubule configuration correlate with nuclear migration in the preblastoderm *Drosophila* embryo. *J. Cell Biol.* 122:113–121. http://dx.doi.org/10.1083/jcb.122.1.113

Baluska, F., D. Volkmann, and P.W. Barlow. 2004. Eukaryotic cells and their cell bodies: Cell Theory revised. *Ann. Bot. (Lond.).* 94:9–32. http://dx.doi.org/10.1093/aob/mch109

Basto, R., J. Lau, T. Vinogradova, A. Gardiol, C.G. Woods, A. Khodjakov, and J.W. Raff. 2006. Flies without centrioles. *Cell.* 125:1375–1386. http://dx.doi.org/10.1016/j.cell.2006.05.025

Bearer, E.L. 1991. Actin in the *Drosophila* embryo: Is there a relationship to developmental cue localization? *Bioessays.* 13:199–204. http://dx.doi.org/10.1002/bies.950130410

Brust-Mascher, I., and J.M. Scholey. 2007. Mitotic spindle dynamics in *Drosophila*. *Int. Rev. Cytol.* 259:139–172. http://dx.doi.org/10.1016/S0074-7696(06)59004-7

Bull, A.L. 1982. Stages of living embryos in the jewel wasp *Mormoniella* (*nasonia*) *vitripennis* (*walker*)(hymenoptera: pteromalidae). *Int. J. Insect Morphol. Embryol.* 11:1–23. http://dx.doi.org/10.1016/0020-7322(82)90034-4

Callaini, G., and M.G. Riparbelli. 1990. Centriole and centrosome cycle in the early *Drosophila* embryo. *J. Cell Sci.* 97:539–543.

Callaini, G., R. Dallai, and M.G. Riparbelli. 1992. Cytochalasin induces spindle fusion in the syncytial blastoderm of the early *Drosophila* embryo. *Biol. Cell.* 74:249–254. http://dx.doi.org/10.1016/0248-4900(92)90035-Y

de Saint Phalle, B., and W. Sullivan. 1996. Incomplete sister chromatid separation is the mechanism of programmed chromosome elimination during early *Sciara coprophila* embryogenesis. *Development*. 122:3775–3784.

Dix, C.I., and J.W. Raff. 2007. *Drosophila* Spd-2 recruits PCM to the sperm centriole, but is dispensable for centriole duplication. *Curr. Biol.* 17: 1759–1764. http://dx.doi.org/10.1016/j.cub.2007.08.065

Field, C.M., and P. Lénárt. 2011. Bulk cytoplasmic actin and its functions in meiosis and mitosis. *Curr. Biol.* 21:R825–R830. http://dx.doi.org/10.1016/j.cub.2011.07.043

Fleig, R., and K. Sander. 1986. Embryogenesis of the honeybee *apis mellifera* I. (hymenoptera: apidae): An sem study. *Int. J. Insect Morphol. Embryol.* 15:449–462. http://dx.doi.org/10.1016/0020-7322(86)90037-1

Foe, V.E., and B.M. Alberts. 1983. Studies of nuclear and cytoplasmic behaviour during the five mitotic cycles that precede gastrulation in *Drosophila* embryogenesis. *J. Cell Sci.* 61:31–70.

Foe, V.E., G.M. Odell, and B.A. Edgar. 1993. Mitosis and morphogenesis in the *Drosophila* embryo: Point and counterpoint. *In* The Development of *Drosophila melanogaster*. M. Bate and A. Martínez-Arias, editors. Cold Spring Harbor Laboratory Press, Cold Spring Harbor, NY. 149–300.

Foe, V.E., C.M. Field, and G.M. Odell. 2000. Microtubules and mitotic cycle phase modulate spatiotemporal distributions of F-actin and myosin II in *Drosophila* syncytial blastoderm embryos. *Development*. 127:1767–1787.

Freeman, M., C. Nüsslein-Volhard, and D.M. Glover. 1986. The dissociation of nuclear and centrosomal division in gnu, a mutation causing giant nuclei in *Drosophila*. *Cell*. 46:457–468. http://dx.doi.org/10.1016/0092-8674(86)90666-5

Glotzer, M. 2009. The 3Ms of central spindle assembly: Microtubules, motors and MAPs. *Nat. Rev. Mol. Cell Biol.* 10:9–20. http://dx.doi.org/10.1038/nrm2609

Gönczy, P. 2008. Mechanisms of asymmetric cell division: Flies and worms pave the way. *Nat. Rev. Mol. Cell Biol.* 9:355–366. http://dx.doi.org/10.1038/nrm2388

Grill, S.W., and A.A. Hyman. 2005. Spindle positioning by cortical pulling forces. *Dev. Cell.* 8:461–465. http://dx.doi.org/10.1016/j.devcel.2005.03.014

Grill, S.W., J. Howard, E. Schäffer, E.H. Stelzer, and A.A. Hyman. 2003. The distribution of active force generators controls mitotic spindle position. *Science*. 301:518–521. http://dx.doi.org/10.1126/science.1086560

Hamaguchi, M.S., and Y. Hiramoto. 1986. Analysis of the Role of Astral Rays in Pronuclear Migration in Sand Dollar Eggs by the Colcemid-UV Method. *Dev. Growth Differ.* 28:143–156. http://dx.doi.org/10.1111/j.1440-169X.1986.00143.x

Hatanaka, K., and M. Okada. 1991. Retarded nuclear migration in *Drosophila* embryos with aberrant F-actin reorganization caused by maternal mutations and by cytochalasin treatment. *Development*. 111:909–920.

Karpova, N., Y. Bobinnec, S. Fouix, P. Huitorel, and A. Debec. 2006. Jupiter, a new *Drosophila* protein associated with microtubules. *Cell Motil. Cytoskeleton*. 63:301–312. http://dx.doi.org/10.1002/cm.20124

Kellogg, D.R., T.J. Mitchison, and B.M. Alberts. 1988. Behaviour of microtubules and actin filaments in living *Drosophila* embryos. *Development*. 103:675–686.

Markow, T.A., S. Beall, and L.M. Matzkin. 2009. Egg size, embryonic development time and ovoviviparity in *Drosophila* species. *J. Evol. Biol.* 22:430–434. http://dx.doi.org/10.1111/j.1420-9101.2008.01649.x

Mazia, D. 1993. The cell cycle at the cellular level. *Eur. J. Cell Biol.* 61:14.

Mazumdar, A., and M. Mazumdar. 2002. How one becomes many: Blastoderm cellularization in *Drosophila melanogaster*. *Bioessays*. 24:1012–1022. http://dx.doi.org/10.1002/bies.10184

Megraw, T.L., K. Li, L.R. Kao, and T.C. Kaufman. 1999. The centrosomin protein is required for centrosome assembly and function during cleavage in *Drosophila*. *Development*. 126:2829–2839.

Megraw, T.L., L.R. Kao, and T.C. Kaufman. 2001. Zygotic development without functional mitotic centrosomes. *Curr. Biol.* 11:116–120. http://dx.doi.org/10.1016/S0960-9822(01)00017-3

Morin, X., R. Daneman, M. Zavortink, and W. Chia. 2001. A protein trap strategy to detect GFP-tagged proteins expressed from their endogenous loci in *Drosophila*. *Proc. Natl. Acad. Sci. USA*. 98:15050–15055. http://dx.doi.org/10.1073/pnas.261408198

Perondini, A.L.P., H.O. Gutzeit, and L. Mori. 1986. Nuclear division and migration during early embryogenesis of *Bradysia tritici* coquillet (syn. *Sciara ocellaris*) (diptera: Sciaridae). *Int. J. Insect Morphol. Embryol.* 15:155–163. http://dx.doi.org/10.1016/0020-7322(86)90054-1

Pignoni, F., and S.L. Zipursky. 1997. Induction of *Drosophila* eye development by decapentaplegic. *Development*. 124:271–278.

Raff, J.W., and D.M. Glover. 1989. Centrosomes, and not nuclei, initiate pole cell formation in *Drosophila* embryos. *Cell*. 57:611–619. http://dx.doi.org/10.1016/0092-8674(89)90130-X

Raminani, L.N., and E.W. Cupp. 1975. Early embryology of *Aedes aegypti* (L.) (Diptera: Culicidae). *Int. J. Insect Morphol. Embryol.* 4:517–528. http://dx.doi.org/10.1016/0020-7322(75)90028-8

Reinsch, S., and P. Göncizy. 1998. Mechanisms of nuclear positioning. *J. Cell Sci.* 111:2283–2295.

Riparbelli, M.G., G. Callaini, and E.D. Schejter. 2007. Microtubule-dependent organization of subcortical microfilaments in the early *Drosophila* embryo. *Dev. Dyn.* 236:662–670. http://dx.doi.org/10.1002/dvdy.21062

Rodrigues-Martins, A., M. Riparbelli, G. Callaini, D.M. Glover, and M. Bettencourt-Dias. 2007. Revisiting the role of the mother centriole in centriole biogenesis. *Science*. 316:1046–1050. http://dx.doi.org/10.1126/science.1142950

Rodrigues-Martins, A., M. Riparbelli, G. Callaini, D.M. Glover, and M. Bettencourt-Dias. 2008. From centriole biogenesis to cellular function: centrioles are essential for cell division at critical developmental stages. *Cell Cycle*. 7:11–16. http://dx.doi.org/10.4161/cc.7.1.5226

Schejter, E.D., and E. Wieschaus. 1993. Functional elements of the cytoskeleton in the early *Drosophila* embryo. *Annu. Rev. Cell Biol.* 9:67–99. http://dx.doi.org/10.1146/annurev.cb.09.110193.000435

Schenk, C., H. Bringmann, A.A. Hyman, and C.R. Cowan. 2010. Cortical domain correction repositions the polarity boundary to match the cytokinesis furrow in *C. elegans* embryos. *Development*. 137:1743–1753. http://dx.doi.org/10.1242/dev.040436

Schubiger, G., and B. Edgar. 1994. Using inhibitors to study embryogenesis. *Methods Cell Biol.* 44:697–713. http://dx.doi.org/10.1016/S0091-679X(08)60939-1

Sharp, D.J., H.M. Brown, M. Kwon, G.C. Rogers, G. Holland, and J.M. Scholey. 2000. Functional coordination of three mitotic motors in *Drosophila* embryos. *Mol. Biol. Cell*. 11:241–253.

Simonnet, C., and A. Groisman. 2006. High-throughput and high-resolution flow cytometry in molded microfluidic devices. *Anal. Chem.* 78:5653–5663. http://dx.doi.org/10.1021/ac060340o

Sommer, R., and D. Tautz. 1991. Asynchronous mitotic domains during blastoderm formation in *Musca domestica* L. (Diptera). *Rouxs Arch. Dev. Biol.* 199:373–376. http://dx.doi.org/10.1007/BF01705931

Vaizel-Ohayon, D., and E.D. Schejter. 1999. Mutations in centrosomin reveal requirements for centrosomal function during early *Drosophila* embryogenesis. *Curr. Biol.* 9:889–898. http://dx.doi.org/10.1016/S0960-9822(99)80393-5

von Dassow, G., and G. Schubiger. 1994. How an actin network might cause fountain streaming and nuclear migration in the syncytial *Drosophila* embryo. *J. Cell Biol.* 127:1637–1653. http://dx.doi.org/10.1083/jcb.127.6.1637

von Dassow, G., K.J. Verbrugghe, A.L. Miller, J.R. Sider, and W.M. Bement. 2009. Action at a distance during cytokinesis. *J. Cell Biol.* 187:831–845. http://dx.doi.org/10.1083/jcb.200907090

Waterman-Storer, C., D.Y. Duey, K.L. Weber, J. Keech, R.E. Cheney, E.D. Salmon, and W.M. Bement. 2000. Microtubules remodel actomyosin networks in *Xenopus* egg extracts via two mechanisms of F-actin transport. *J. Cell Biol.* 150:361–376. http://dx.doi.org/10.1083/jcb.150.2.361

Wühr, M., Y. Chen, S. Dumont, A.C. Groen, D.J. Needleman, A. Salic, and T.J. Mitchison. 2008. Evidence for an upper limit to mitotic spindle length. *Curr. Biol.* 18:1256–1261. http://dx.doi.org/10.1016/j.cub.2008.07.092

Wühr, M., E.S. Tan, S.K. Parker, H.W. Detrich III, and T.J. Mitchison. 2010. A model for cleavage plane determination in early amphibian and fish embryos. *Curr. Biol.* 20:2040–2045. http://dx.doi.org/10.1016/j.cub.2010.10.024

Zalokar, M., and I. Erk. 1976. Division and migration of nuclei during early embryogenesis of *Drosophila melanogaster*. *J. Microsc. Biol. Cell.* 25:97–106.